CHAPTER 7

REFLECTOR ANTENNAS

7.1 INTRODUCTION

The radiation pattern of a radiating antenna element is modified using reflectors. A simple example is that the backward radiation from an antenna may be eliminated with a large metallic plane sheet reflector. So, the desired characteristics may be produced by means of a large, suitably shaped, and illuminated reflector surface. The characteristics of antennas with sheet reflectors or their equivalent are considered in this chapter.

Some reflectors are illustrated in Figure 7.1. The arrangement in Figure 7.1a has a large, flat sheet reflector near a linear dipole antenna to reduce the backward radiation. With small spacing between the antenna and sheet this arrangement also yields an increase in substantial gain in the forward radiation. The desirable properties of the sheet reflector may be largely preserved with the reflector reduced in size as long as its size is greater than that of the antenna.

With two flat sheets intersecting at an angle α ($<180^\circ$) as in Figure 7.1b, a sharper radiation pattern than from a flat sheet reflector ($\alpha = 180^\circ$) can be obtained. This arrangement, called *corner reflector antenna*, is most practical where apertures of 1 or 2λ are of convenient size. A corner reflector without an exciting antenna can be used as a *passive reflector* or target for radar waves. In this application the aperture may be many wavelengths, and the corner angle is *always* 90°. Reflectors with this angle have the property that an incidence wave is reflected back toward its source, the corner acting as a *retroreflector*.

When it is feasible to build antennas with apertures of many wavelengths, parabolic reflectors can be used to provide highly directional antennas. A parabolic reflector antenna is shown in Figure 7.1c. The parabola reflects the waves originating from a source at the focus into a parallel beam, the parabola transforming the curved wave front from the feed antenna at the focus into a plane wave front. A front fed and a cassegrain – feed parabolic reflectors are depicted in Figures 7.1c and d. Many other shapes of reflectors can be employed for special applications. For instance, with an antenna at one focus, the elliptical reflector produces a diverging beam with all reflected waves passing through the second focus of the ellipse. Examples of reflectors of other shapes are the hyperbolic and the spherical reflectors.

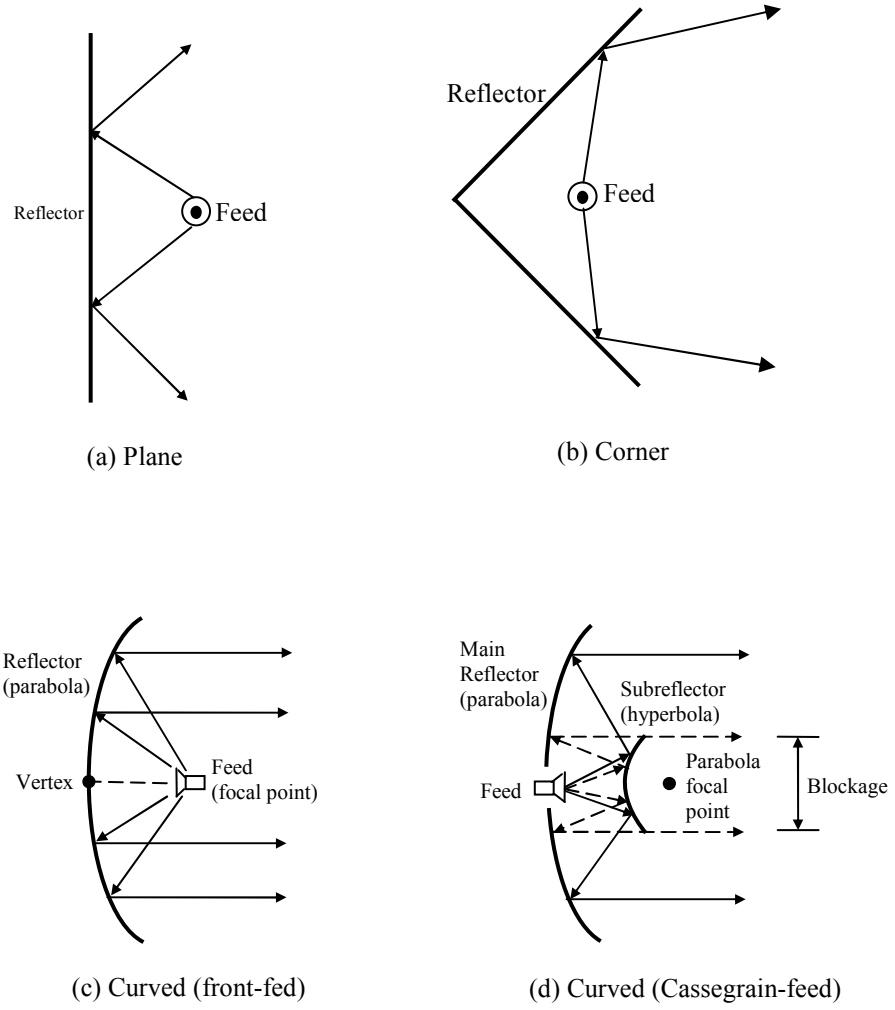

Figure 7.1 Some configurations of reflector antennas

The plane sheet reflector, the corner reflector, the parabolic reflector and other reflectors are discussed in more detail in the following sections. In addition, feed systems, aperture blockage, aperture efficiency, diffraction, surface irregularities, gain and frequency-selective surfaces are considered.

7.2 PLANE REFLECTORS

Let an omnidirectional antenna is placed at a distance h above an infinite, flat, perfect electric conductor as shown in Figure 7.2. Power from the actual source is radiated in all directions in a manner determined by its unbounded medium directional properties. For an observation point p_1, there is a direct wave. In addition, a wave from the actual source radiated toward point R_1 of the interface undergoes a reflection. The direction is determined by the law of reflection $\left(\theta_1^i = \theta_1^r\right)$ which assures that the energy in

homogeneous media travels in straight lines along the shortest paths. This wave will pass through the observation point p_1. By extending its actual path below the interface, it will seem to originate from a virtual source positioned a distance h below the boundary. For another observation point p_2 the point of reflection is R_2, but the virtual source is the same as before. The same is concluded for all other observation points above the interface.

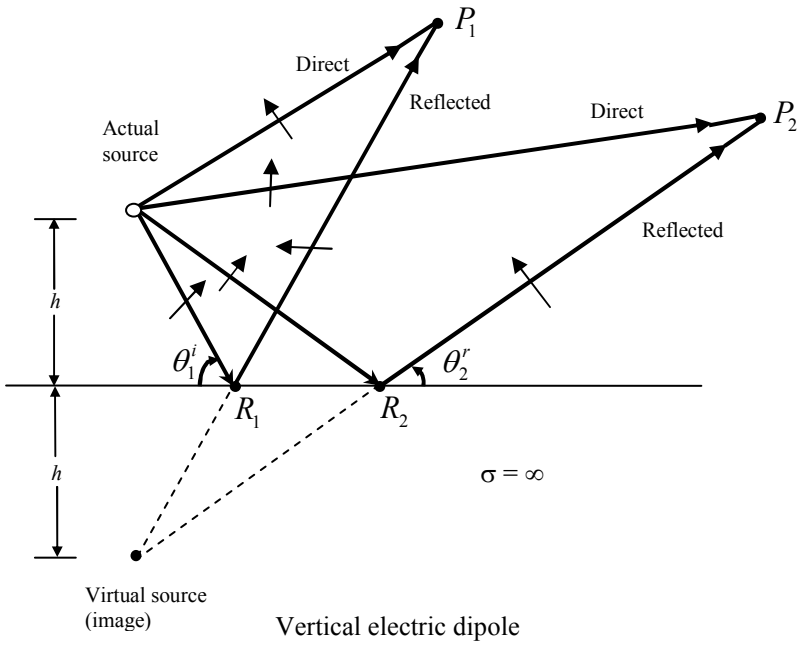

Figure 7.2 Antenna above an infinite, flat, perfect electric conductor.

The amount of reflection is generally determined by the respective constitutive parameters of the media below and above the interface. For a perfect electric conductor below the interface, the incidence wave is completely reflected and the field below the boundary is zero. According to the boundary conditions, the tangential components of the electric field must vanish at all points along the interface. Thus for an incident electric field with vertical polarization shown by the arrows, the polarization of the reflected waves must be as indicated in the figure to satisfy the boundary conditions.

For a vertical dipole, to excite the polarization of the reflected waves, the virtual source must also be vertical and with a polarity in the same direction as that of the actual source (thus a reflection coefficient of +1). Another orientation of the source will be to have the radiating element in a horizontal position, as shown in Figure 7.3. As shown in Figures 7.3, the virtual source (image) is also placed at a distance h below the interface. For horizontal polarized antenna, the image will have a 180° polarity difference relative to the actual source (thus a reflection coefficient of -1).

In addition to electric sources, artificial equivalent "magnetic" sources have been introduced to aid in the analyses of electromagnetic boundary value problems. Figure 7.3 displays the sources and their images for an electric plane conductor. The single arrow indicates an electric element and the double a magnetic one. The direction of the arrow identifies the polarity.

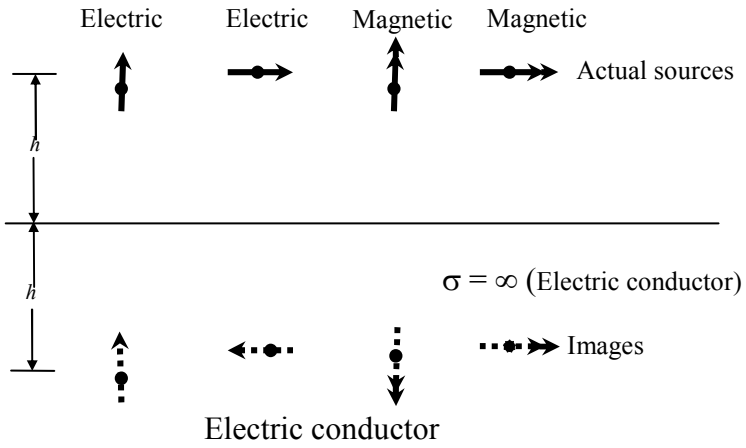

Figure 7.3 Electric and magnetic sources and their images near electric conductors.

7.2.1 Vertical Electric Dipole

The analysis procedure for vertical and horizontal electric and magnetic elements near infinite electric plane conductors, using image theory, was illustrated graphically in the previous section. Based on the graphical model of Figure 7.2, the mathematical expressions for the fields of a vertical linear element near a perfect electric conductor will now be developed. For simplicity, only far-field observations will be considered.

Referring to the geometry of Figure 7.4(a), the far-zone direct component of the electric field of the infinitesimal dipole of length l, constant current I_0, and observation point P is given by

$$E_\theta^{\,d} \;\square\; j\eta \frac{kI_0 l e^{-jkr_1}}{4\pi r_1} \sin\theta_1 \tag{7.1}$$

The reflected component can be accounted for by the introduction of the virtual source (image) as shown in Figure 7.4(a), and it can be written as

$$E_\theta^r = jR_v \eta \frac{kI_0 l e^{-jkr_2}}{4\pi r_2} \sin\theta_2 \tag{7.2}$$

or

$$E_\theta^r = j\eta \frac{kI_0 l e^{-jkr_2}}{4\pi r_2} \sin\theta_2 \tag{7.2a}$$

Since the reflection coefficient R_v is equal to unity.

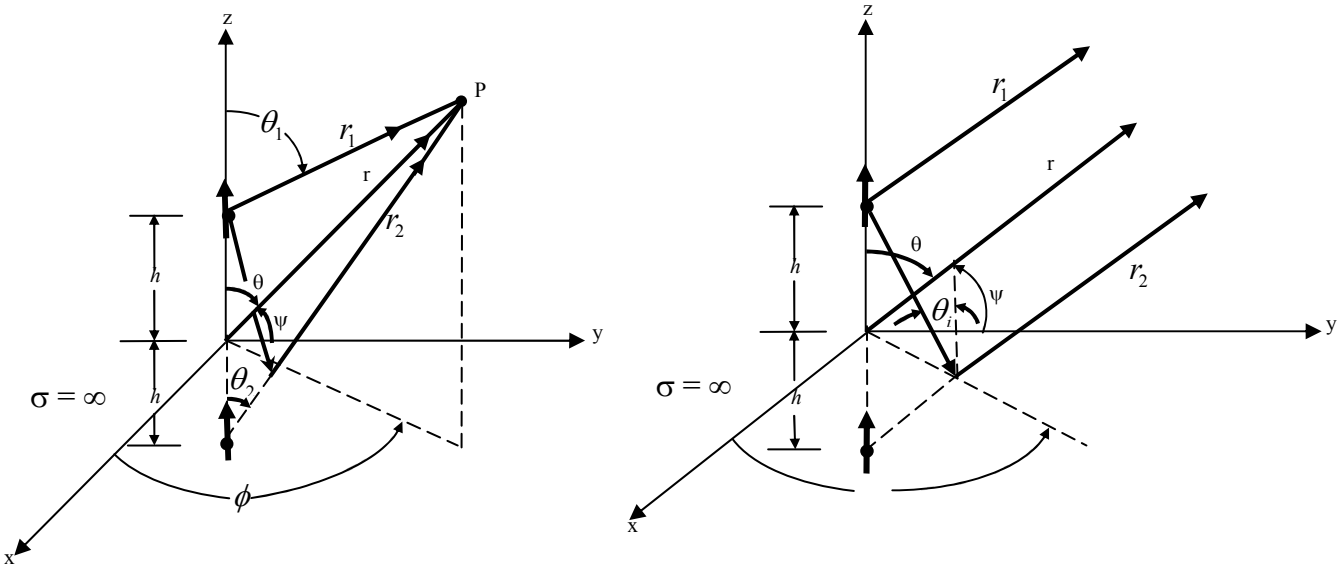

Figure 7.4 (a) Vertical electric dipole above infinite perfect electric conductor and its (b) Far-field observations

The total field above the interface (z ≥ 0) is equal to the sum of the direct and reflected components as given by (7.1) and (7.2a). Since a field cannot exist inside a perfect electric conductor, it is equal to zero below the interface. To simplify the expression for the total electric field, it is referred to the origin of the coordinate system (z = 0).

In general, we can write that

$$r_1 = \left[r^2 + h^2 - 2rh\cos\theta \right]^{1/2} \tag{7.3a}$$

$$r_2 = \left[r^2 + h^2 - 2rh\cos(\pi - \theta) \right]^{1/2} \tag{7.3b}$$

For far-field observations $(r \gg h)$, (7.3a) and (7.3b) reduce using the binomial expansion to

$$r_1 \approx r - h\cos\theta \tag{7.4a}$$

$$r_2 \approx r + h\cos\theta \tag{7.4b}$$

As shown in Figure 7.4(b), geometrically (7.4a) and (7.4b) represent parallel lines. Since the amplitude variations are not as critical

$$r_1 \approx r_2 \approx r \qquad \text{for amplitude variations} \tag{7.5}$$

Using (7.4a)-(7.5), the sum of (7.1) and (7.2a) can be written as

$$\left.\begin{aligned} E_\theta &\approx j\eta \frac{kI_0 l e^{-jkr_2}}{4\pi r} \sin\theta \left[2\cos\left(kh\cos\theta\right)\right] && z \geq 0 \\ E_\theta &= 0 && z < 0 \end{aligned}\right\} \tag{7.6}$$

The shape and amplitude of the field is not only controlled by the field of the single element but also by the positioning of the element relative to the ground. To examine the field variations as a function of the height h, the normalized (to 0 dB) power patterns for h = 0, λ/8, λ/4, 3λ/8, λ/2, and λ are plotted in Figure 7.5. Because of symmetry, only half of each pattern is shown. For $h > \lambda/4$ more minor lobes, in addition to the major ones, are formed. As h attains values greater than λ, an even greater number of minor lobes are introduced. The introduction of the additional lobes is usually called scalloping. In general, the total number of lobes is equal to the integer that is close to

$$number\ of\ lobes \approx \frac{2h}{\lambda} + 1 \tag{7.7}$$

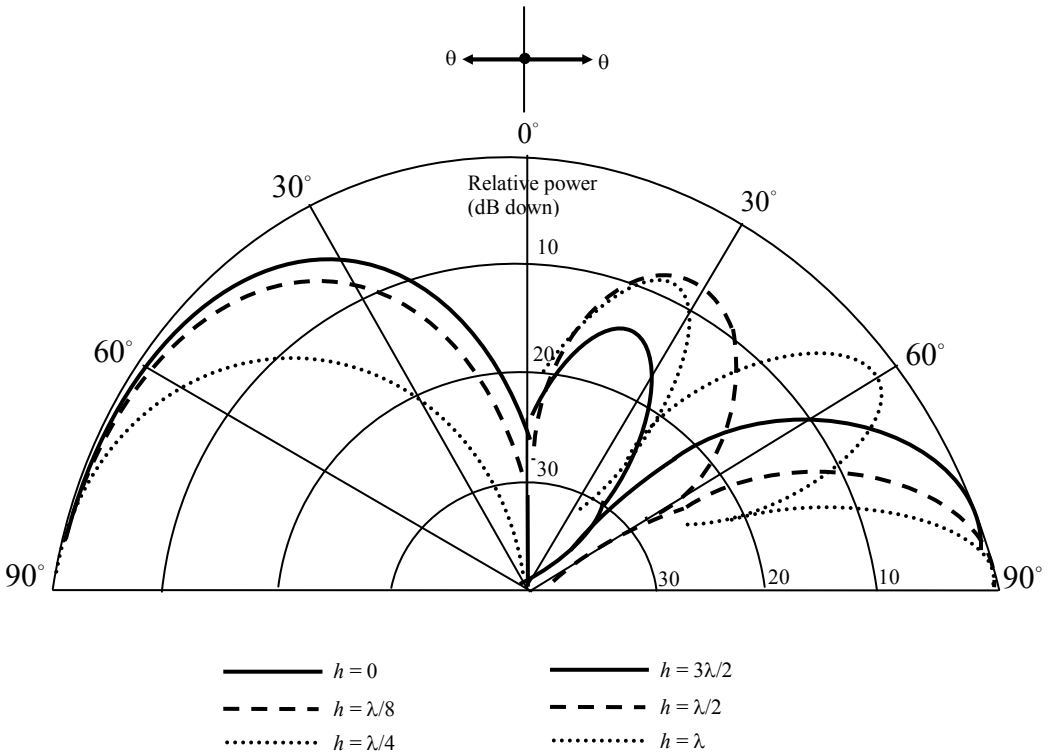

Figure 7.5 Elevation plane amplitude patterns of a vertical infinitesimal electric dipole for different heights above an infinite perfect electric conductor.

Since the total field of the antenna system is different from that of a singe element, the directivity and radiation resistance are also different. The directivity can be written as

$$D_0 = \frac{4\pi U_{\max}}{\mathrm{P}_{\mathrm{r}\,ad}} = \frac{2}{\left[\dfrac{1}{3} - \dfrac{\cos(2kh)}{(2kh)^2} + \dfrac{\sin(2kh)}{(2kh)^3}\right]} \tag{7.8}$$

Whose value for $kh = 0$ is 3. The maximum value occurs when $kh = 2.881$ ($h = 0.4585\lambda$), and it is equal to 6.566 which is greater than four times that of an isolated dipole element (1.5). The directivity is displayed in Figure 7.6 for $0 \le h \le 5\lambda$.

Similarly, from radiated power, the radiation resistance can be written as

$$R_r = \frac{2P_{rad}}{\left|I_0\right|^2} = 2\pi\eta\left(\frac{l}{\lambda}\right)^2\left[\frac{1}{3} - \frac{\cos(2kh)}{(2kh)^2} + \frac{\sin(2kh)}{(2kh)^3}\right] \tag{7.9}$$

Whose value for $kh \to \infty$ is the same and for $kh = 0$ is twice that of the isolated element as given by (7.9). When $kh = 0$, the value of R_r is only one-half the value of an $l' = 2l$ isolated element.

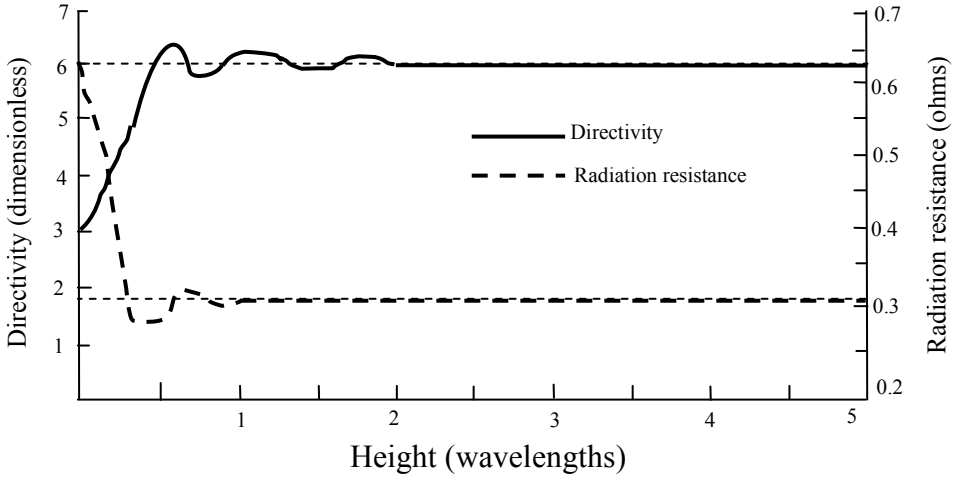

Figure 7.6 Directivity and radiation resistance of a vertical infinitesimal electric dipole as a function of its height above an infinite perfect electric conductor.

7.2.2 Horizontal Electric Dipole

Another dipole configuration is when the linear element is placed horizontally relative to the infinite electric ground plane, as shown in Figure 7.7. The analysis procedure of this is identical to the one of the vertical dipole. Introducing an image and assuming far-field observations, as shown in Figure 7.7(a, b), the direct component can be written as

$$E_{\psi}^{d} \; \square \; j\eta \frac{kI_0 l e^{-jkr_1}}{4\pi r_1} \sin\psi \tag{7.10}$$

and the reflected one by

$$E_{\psi}^{r} = jR_h \eta \frac{kI_0 l e^{-jkr_2}}{4\pi r_2} \sin\psi \tag{7.11}$$

or

$$E_{\psi}^{r} = -j\eta \frac{kI_0 l e^{-jkr_2}}{4\pi r_2} \sin\psi \tag{7.11a}$$

since the reflection coefficient is equal to $R_h = -1$.

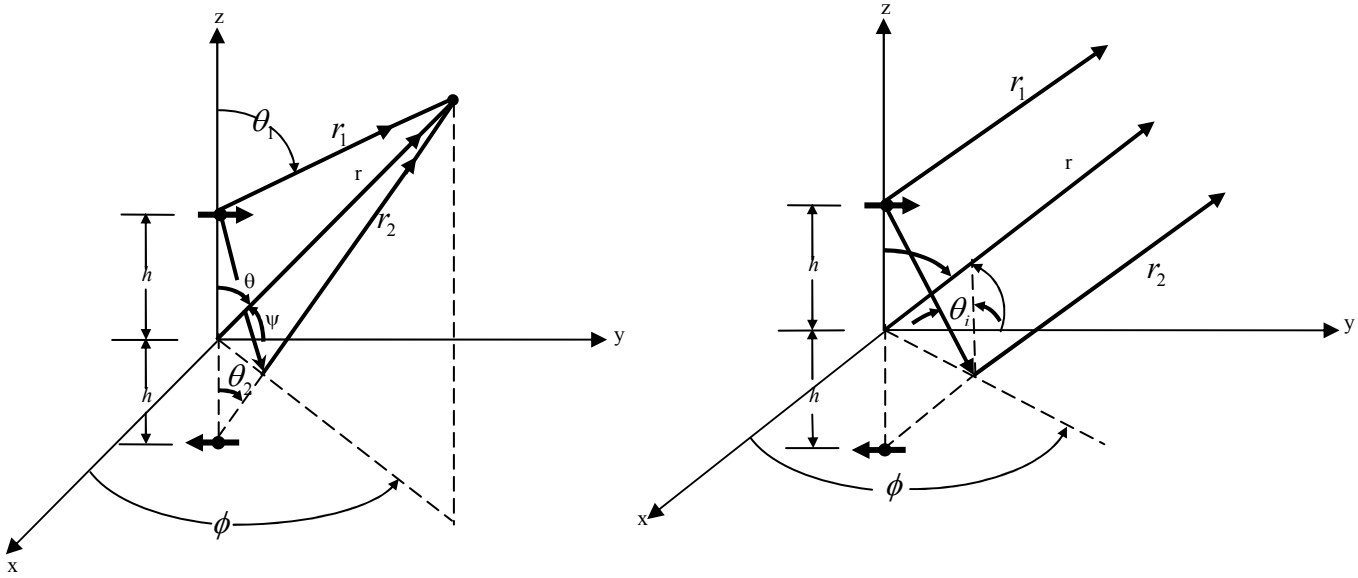

Figure 7.7 Horizontal electric dipole above an infinite perfect electric conductor and its far-field observations.

To find the angle ψ, which is measured from the y-axis toward the observation point, we first form

$$\cos\psi = \hat{a}_y . \hat{a}_r = \hat{a}_y . (\hat{a}_x \sin\theta\cos\phi + \hat{a}_y \sin\theta\sin\phi + \hat{a}_z \cos\theta) = \sin\theta\sin\phi \tag{7.12}$$

from which we find

$$\sin\psi = \sqrt{1-\cos^2\psi} = \sqrt{1-\sin^2\theta\sin^2\phi} \tag{7.13}$$

Since for far-field observations

$$\left.\begin{aligned} r_1 &\approx r - h\cos\theta \\ r_2 &\approx r + h\cos\theta \end{aligned}\right\} \quad \text{for phase variations} \tag{7.14a}$$

$$r_1 \approx r_2 \approx r \quad \text{for amplitude variations} \tag{7.14b}$$

The total field, which is valid only above the ground plane $\left(z \geq 0; 0 \leq \theta \leq \pi/2, 0 \leq \phi \leq 2\pi\right)$, can be written as

$$E_\psi = E_\psi^d + E_\psi^r = j\eta \frac{kI_0 l e^{-jkr_1}}{4\pi r} \sqrt{1 - \sin^2\theta \sin^2\phi} \left[2j \sin\left(kh\cos\theta\right)\right] \tag{7.15}$$

Equation (7.15) again consists of the product of the field of a single isolated element placed symmetrically at the origin and a factor (within the brackets) known as the array factor. This again is the pattern multiplication rule.

To examine the variations of the total field as a function of the element height above the ground plane, the two dimensional elevation plane patterns (normalized to 0 dB) for $\phi = 90^\circ$ (y-z plane) when h = 0, λ/8, λ/4, 3λ/8, λ/2, and λ are plotted in Figure 7.8. Since this antenna system is not symmetric, the azimuthal plane (x-y plane) pattern will not be isotropic.

As the height increases beyond one wavelength (h > λ), a larger number of lobes is again formed. The total number of lobes is equal to the integer that most closely is equal to

$$number\ of\ lobes \approx 2\left(\frac{h}{\lambda}\right) \tag{7.16}$$

With unity being the smallest number.

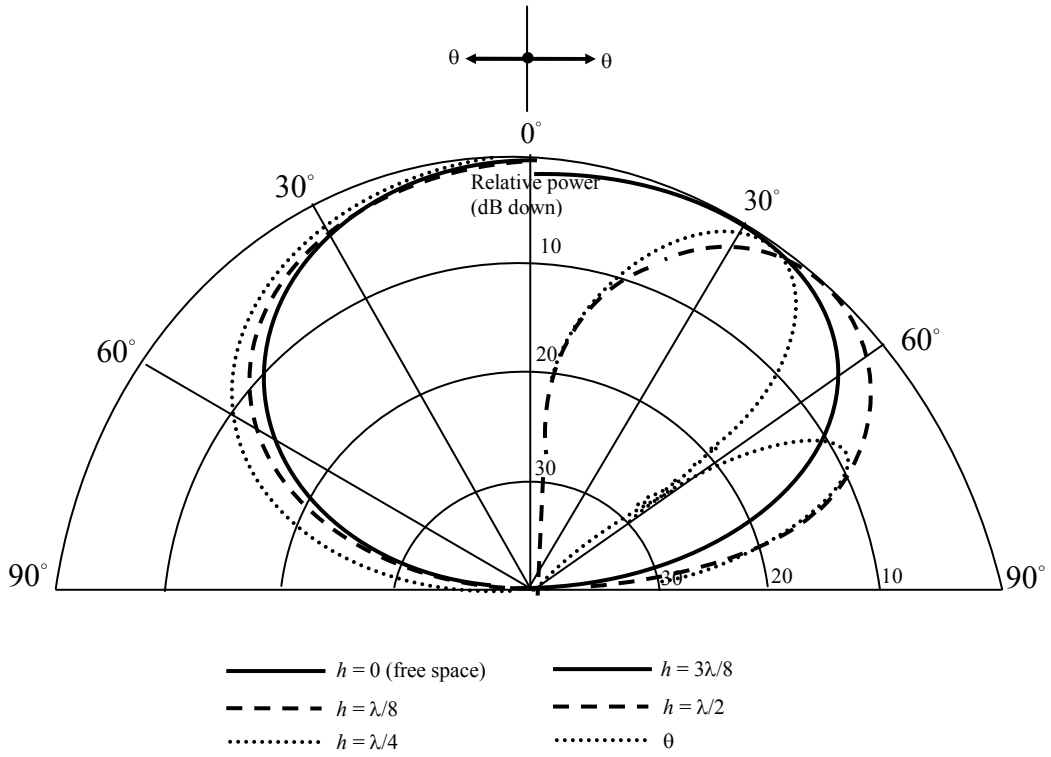

Figure 7.8 Elevation plane $\left(\phi = 90^{\circ}\right)$ amplitude patterns of a horizontal infinitesimal electric dipole for different heights above an infinite perfect electric conductor.

The directivity can be written as

$$D_0 = \frac{4\pi U_{\max}}{\mathrm{P}_{\mathrm{r}\,ad}} = \begin{cases} \dfrac{4\sin^2(kh)}{R(kh)} & kh \le \pi/2 \left(h \le \lambda/4\right) \quad (7.17a) \\ \dfrac{4}{R(kh)} & kh \ge \pi/2 \left(h > \lambda/4\right) \quad (7.17b) \end{cases}$$

where

$$R(kh) = \left[\frac{2}{3} - \frac{\sin(2kh)}{2kh} - \frac{\cos(2kh)}{(2kh)^2} + \frac{\sin(2kh)}{(2kh)^3}\right] \quad (7.17c)$$

For small values of $kh\left(kh \to 0\right)$, (7.17a) reduces to

$$D_0 = \frac{4\sin^2(kh)}{\left[\dfrac{2}{3} - \dfrac{2}{3} + \dfrac{8}{15}(kh)^2\right]} = 7.5\left(\frac{\sin kh}{kh}\right)^2 \quad (7.18)$$

For h = 0 the element is shorted and it does not radiate. The directivity is plotted for $0 \le h \le 5\lambda$ in Figure 7.9. It exhibits a maximum value of 7.5 for small values of h. A values of 6 occurs when $h \approx (0.725 + n/2)\lambda$, n = 1, 2, 3,…

The conductivity has a more pronounced effect on the impedance values, compared to those of the vertical dipole on input impedance. The values of the resistance and reactance approach, as the height increases, to the corresponding values of the isolated element of length λ/2 (73 ohms for the resistance and 42.5 ohms for the reactance).

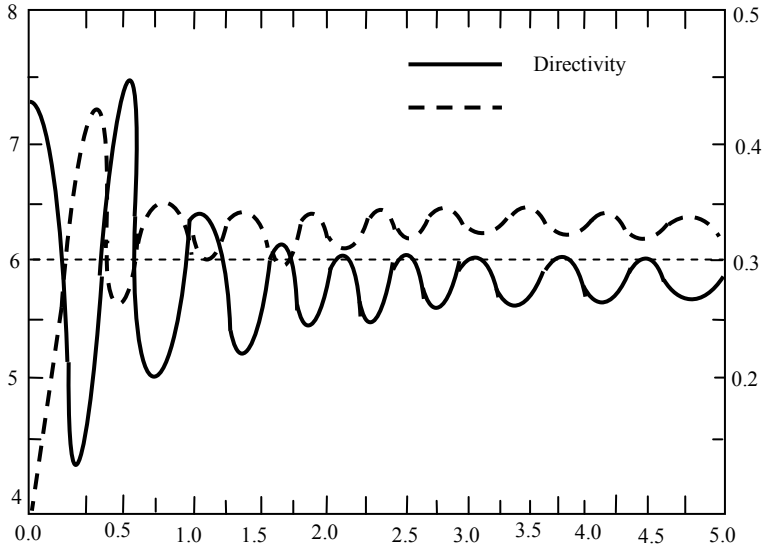

Figure 7.9 Radiation resistance and directivity of a horizontal infinitesimal electric dipole as a function of its height above an infinite perfect electric conductor.

7.3 CORNER REFLECTOR

For better collimination of the power in the forward directions, an arrangement can be made with two plane reflectors joined so as to form a corner, as shown in Figure 7.10 (a). This is known as the corner reflector. Because of its simplicity in construction, it has many unique applications. For example, if the reflector is used as a passive target for radar or communication applications, it will return the signal exactly in the same direction as it received it when its included angle is 90°. This is illustrated geometrically in Figure 7.10(b). Because of this unique feature, military ships and vehicles are designed with minimum sharp corners to reduce their detection by enemy radar.

In most practical applications, the included angle formed by the plates is usually 90°; however other angles are also used. To maintain a given system efficiency, the spacing between the vertex and the feed element must increase as the included angle of the reflector decreases, and vice-versa. For reflectors with infinite sides, the gain increases as

the included angle between the planes decreases. This, however, may not be true for finite size plates. For simplicity, in this chapter it will be assumed that the plates themselves are infinite in extent ($l = \infty$). However, since in practice the dimensions must be finite, guidelines on the size of aperture D_a, length (l), height (h) is given.

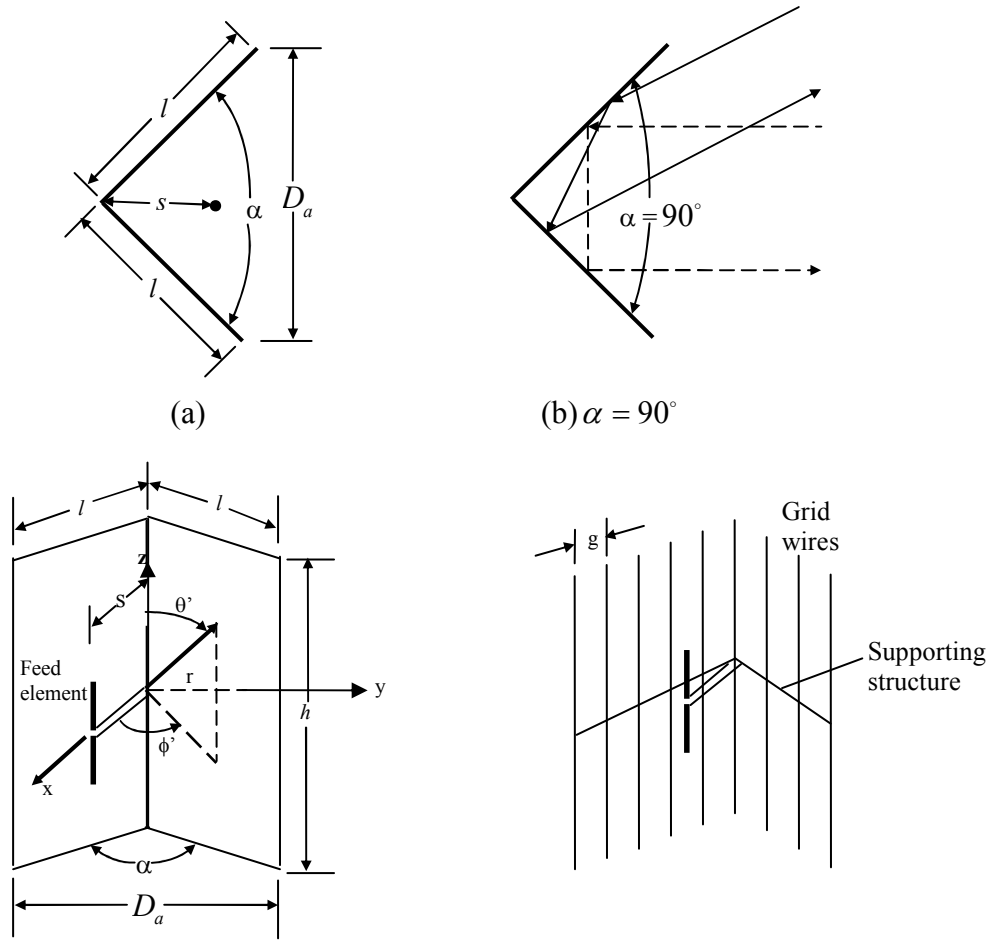

Figure 7.10 Side and perspective views of solid and wire-grid corner reflectors.

The feed element for a corner reflector is almost always a dipole or an array of collinear dipoles placed parallel to the vertex distance s away, as shown in in Figure 7.10 (c). Greater bandwidth is obtained when the feed elements are cylindrical or biconical dipoles instead of thin wires. In many applications, especially when the wavelength is large compared to tolerable physical dimensions, the surfaces of the corner reflector are frequently made of grid wires rather than solid sheet metal, as shown in Figure 7.10 (d). One of the reasons for doing that is to reduce wind resistance and overall system weight. The spacing g between wires is made a small fraction of a wavelength (usually $g \leq \lambda/10$). For wires that are parallel to the length of the dipole, as is the case for the

arrangement of Figure 7.10(d), the reflectivity of the grid-wire surface is as good as that of a solid surface.

In practice, the aperture of the corner reflector (D_a) is usually made between one and two wavelengths $\left(\lambda < D_a < 2\lambda\right)$. The length of the sides of a 90° corner reflector is most commonly taken to be about twice the distance from the vertex to the feed $\left(l \approx 2s\right)$. For reflectors with smaller included angles, the sides are made larger. The feed-to-vertex distance (s) is usually taken to be between $\lambda/3$ and $2\lambda/3$ ($\lambda/3 < s < 2\lambda/3$). For each reflector, there is an optimum feed-to-vertex spacing. If the spacing becomes too small, the radiation resistance decreases and becomes comparable to the loss resistance of the system which leads to an inefficient antenna. For very large spacing, the system produces undesirable multiple lobes, and it loses its directional characteristics. It has been experimentally observed that increasing the size of the sides does not greatly affect the beamwidth and directivity, but it increases the bandwidth and radiation resistance. The main lobe is somewhat broader for reflectors with finite sides compared to that of infinite dimensions. The height (h) of the reflector is usually taken to be about 1.2 to 1.5 times greater than the total length of the feed element, in order to reduce radiation toward the back region from the ends.

The analysis for the field radiated by a source in the presence of a corner reflector is facilitated when the included angle (α) of the reflector is $\alpha = \pi/n$, where n is an integer ($\alpha = \pi, \pi/2, \pi/3, \pi/4$, etc.). For these cases $\left(\alpha = 180^\circ, 90^\circ, 60^\circ, 45^\circ, etc.\right)$ it is possible to find a system of images, which when properly placed in the absence of the reflector plates, form an array that yields the same field within the space formed by the reflector plates as the actual system. The number of images, polarity, and position is controlled by included angle and the polarization of the feed element. The geometrical and electrical arrangement of the images for corner reflectors with included angles of $90^\circ, 60^\circ, 45^\circ \; and \; 30^\circ$ and feed with perpendicular polarization are displayed in Figure 7.11.

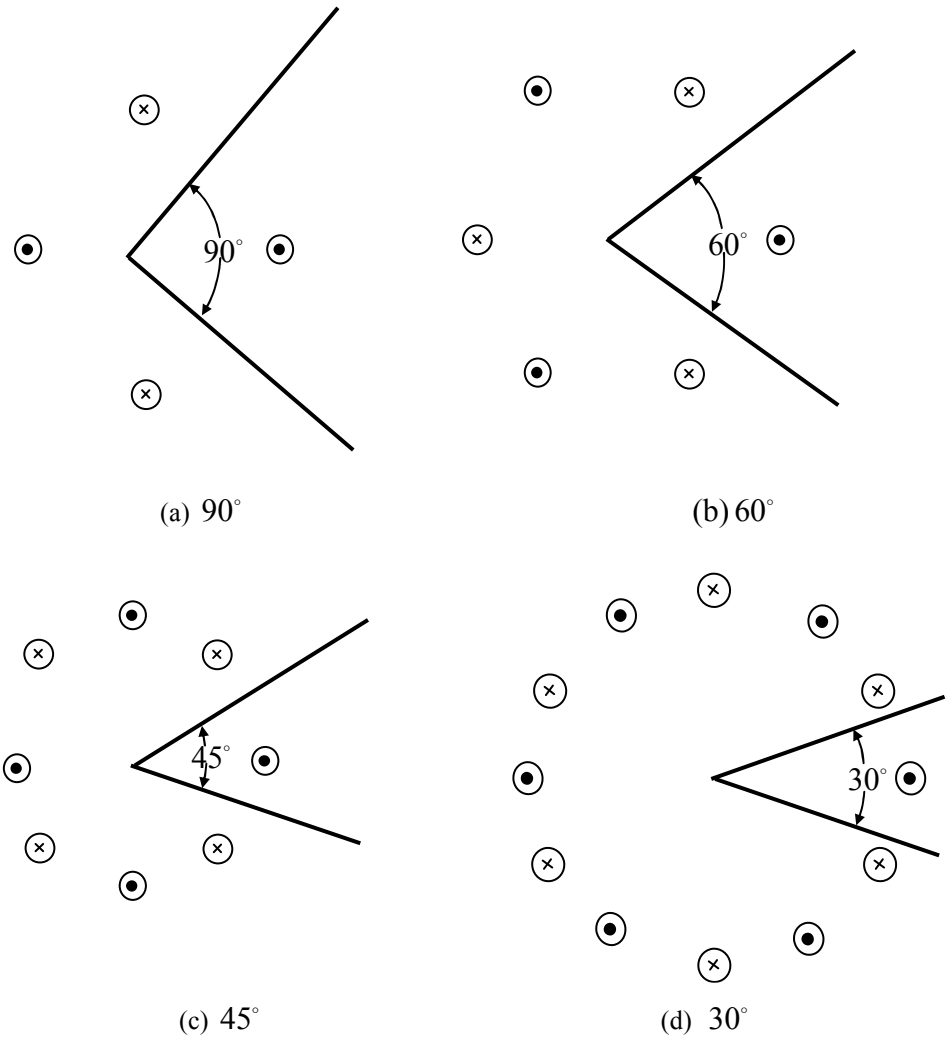

(a) 90° (b) 60°

(c) 45° (d) 30°

Figure 7.11 Corner reflectors and their images (with perpendicularly polarized feeds) for angles of $90^\circ, 60^\circ, 45^\circ$ *and* 30°.

The procedure for finding the number, location, and polarity of the images is demonstrated graphically in Figure 7.12 for a corner reflector with a 90° included angle. It is assumed that the feed element is a linear dipole placed parallel to the vertex. A similar procedure can be followed for all other reflectors with an included angle of $\alpha = 180^\circ/n$, where n is an integer.

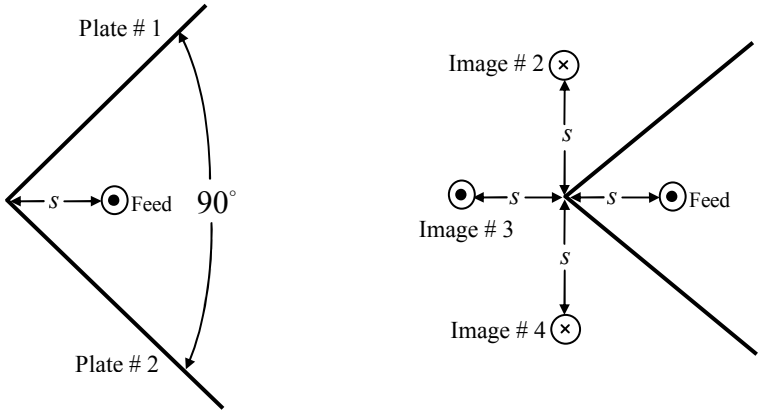

(a) 90° corner reflector

(b) Images for 90° corner reflector

Figure 7.12 Geometrical placement and electrical polarity of images for a 90° corner reflector with a parallel polarized feed.

7.3.1 A 90° Corner Reflector

For the corner reflector with an included angle of 90°, the total field of the system can be derived by summing the contributions from the feed and its images. Thus

$$E(r,\theta,\phi) = E_1(r_1,\theta,\phi) + E_2(r_2,\theta,\phi) + E_3(r_3,\theta,\phi) + E_4(r_4,\theta,\phi) \tag{7.18}$$

In the far-zone, the normalized scalar field can be written as

$$E(r,\theta,\phi) = f(\theta,\phi)\frac{e^{-jkr_1}}{r_1} - f(\theta,\phi)\frac{e^{-jkr_2}}{r_2} + f(\theta,\phi)\frac{e^{-jkr_3}}{r_3} - f(\theta,\phi)\frac{e^{-jkr_4}}{r_4}$$

$$E(r,\theta,\phi) = \left[e^{+jks\cos\psi_1} - e^{+jks\cos\psi_2} + e^{+jks\cos\psi_3} - e^{+jks\cos\psi_4}\right] f(\theta,\phi)\frac{e^{-jkr}}{r} \tag{7.19}$$

where

$$\cos\psi_1 = \hat{a}_x.\hat{a}_r = \sin\theta\cos\phi \tag{7.19a}$$

$$\cos\psi_2 = \hat{a}_y.\hat{a}_r = \sin\theta\,\mathrm{s}in\phi \tag{7.19b}$$

$$\cos\psi_3 = -\hat{a}_x.\hat{a}_r = -\sin\theta\cos\phi \tag{7.19c}$$

$$\cos\psi_4 = -\hat{a}_y.\hat{a}_r = -\sin\theta\sin\phi \tag{7.19d}$$

since $\hat{a}_r = \hat{a}_x \sin\theta\cos\phi + \hat{a}_y \sin\theta\sin\phi + \hat{a}_z \cos\theta$. Equation (7.18) can also be written, using (7.19a)-(7.19d), as

$$E(r,\theta,\phi) = 2\left[\cos(ks\sin\theta\cos\phi) - \cos(ks\sin\theta\sin\phi)\right] f(\theta,\phi)\frac{e^{-jkr}}{r} \tag{7.20}$$

where $0 \le \phi \le \alpha/2 \quad 0 \le \theta \le \pi \quad 2\pi - \alpha/2 \le \phi \le 2\pi$ (7.21a)

Letting the field of a single isolated (radiating in free-space) element to be

$$E_0 = f(\theta,\phi)\frac{e^{-jkr}}{r} \tag{7.22}$$

(7.20) can be rewritten as

$$\frac{E}{E_0} = AF(\theta,\phi) = 2\left[\cos\left(ks\sin\theta\cos\phi\right) - \cos\left(ks\sin\theta\sin\phi\right)\right] \tag{7.23}$$

Equation (7.23) represents not only the ratio of the total field to that of an isolated element at the origin but also the array factor of the entire reflector system. In the azimuthal plane ($\theta = \pi/2$), (7.23) reduces to

$$\frac{E}{E_0} = AF(\theta = \pi/2,\phi) = 2\left[\cos\left(ks\cos\phi\right) - \cos\left(ks\sin\phi\right)\right] \tag{7.24}$$

The normalized patterns for a $\alpha = 90^\circ$ corner reflector for spacings of s = 0.1λ, 0.7λ, 0.8λ, 0.9λ, and 1.0λ is shown in Figure 7.13. It is evident that for the small spacing the pattern consists of a single major lobe whereas multiple lobes appear for the larger spacings (s > 0.7λ). For s = λ the pattern exhibits two lobes separated by a null along the $\phi = 0^\circ$ axis.

Another parameter of performance for the corner reflector is the field strength along the symmetry axis $\left(\theta = 90^\circ, \phi = 0^\circ\right)$ as a function of feed-to-vertex distance s. The normalized (relative to the field of a single isolated element) absolute field strength peaks when s = 0.5λ, and it is equal to 4. The field is also periodic with a period of $\Delta s/\lambda = 1$.

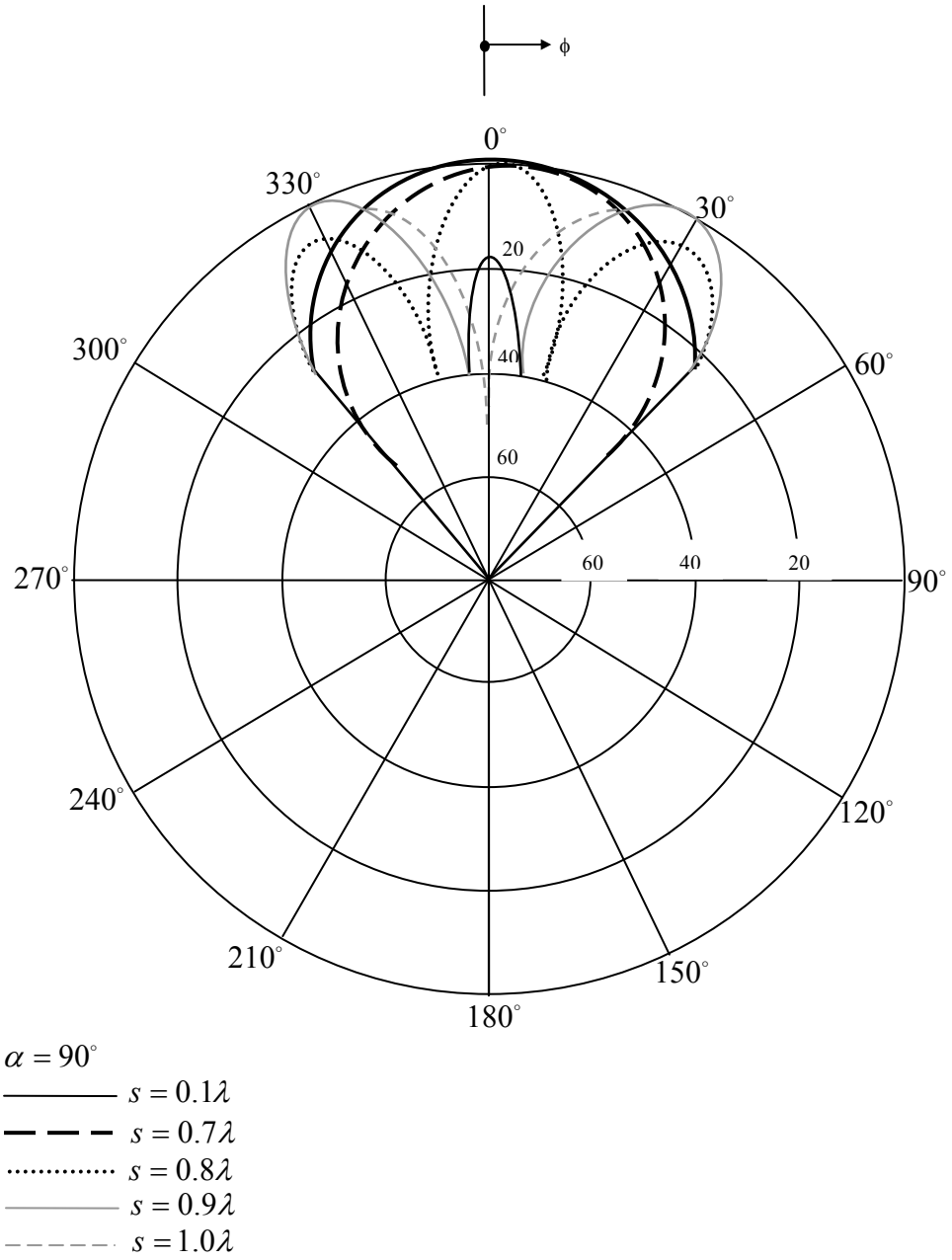

Figure 7.13 Normalized radiation patterns for $\alpha = 90^\circ$ corner reflector for various values of s.

7.3.2 Other Corner Reflectors

A similar procedure can be used to derive the array factors and total fields for all other corner reflectors with included angles of $\alpha = 180^\circ / n$. Referring to Figure 7.11, it can be shown that the array factors for $\alpha = 60^\circ, 45^\circ \; and \; 30^\circ$ can be written as

$$\underline{\alpha = 60^\circ}$$

$$AF(\theta,\phi) = 4\sin\left(\frac{X}{2}\right)\left[\cos\left(\frac{X}{2}\right) - \cos\left(\sqrt{3}\frac{Y}{2}\right)\right] \tag{7.25}$$

$$\underline{\alpha = 45^\circ}$$

$$AF(\theta,\phi) = 2\left[\cos(X) + \cos(Y) - 2\cos\left(\frac{X}{\sqrt{2}}\right)\cos\left(\frac{Y}{\sqrt{2}}\right)\right] \tag{7.26}$$

$$\underline{\alpha = 30^\circ}$$

$$\begin{aligned} AF(\theta,\phi) = 2\Bigg[&\cos(X) - 2\cos\left(\frac{\sqrt{3}}{2}X\right)\cos\left(\frac{Y}{2}\right) \\ &-\cos(Y) + 2\cos\left(\frac{X}{2}\right)\cos\left(\frac{\sqrt{3}}{2}Y\right)\Bigg] \end{aligned} \tag{7.27}$$

where

$$X = ks\sin\theta\cos\phi \tag{7.28}$$

$$Y = ks\sin\theta\sin\phi \tag{7.29}$$

The array factor for a corner reflector has a form that is similar to the array factor for a uniform circular array. This should be expected since the feed sources and their images in Figure 7.11 form a circular array. The number of images increases as the included angle of the corner reflector decreases.

Patterns have been computed for corner reflectors with included angles of $60^\circ, 45^\circ \text{ and } 30^\circ$. It has been found that these corner reflectors have also single-lobed patterns for the smaller values of *s*, and they become narrower as the included angle decreases. Multiple lobes begin to appear when

$$s \approx 0.95\lambda \qquad \text{for} \alpha = 60^\circ$$
$$s \approx 1.2\lambda \qquad \text{for} \alpha = 45^\circ$$
$$s \approx 2.5\lambda \qquad \text{for} \alpha = 30^\circ$$

The maximum field strength increases as the included angle of the reflector decreases. This is expected since a smaller angle reflector exhibits better directional characteristics because of the narrowness of its angle. The maximum values of $|E/E_0|$ for $\alpha = 60^\circ, 45^\circ, \text{and } 30^\circ$ are approximately 5.2, 8, and 9, respectively. The first field strength peak, is achieved when

$$s \approx 0.65\lambda \qquad \text{for} \alpha = 60^\circ$$
$$s \approx 0.85\lambda \qquad \text{for} \alpha = 45^\circ$$

$s \approx 1.20\lambda$ for $\alpha = 30^\circ$

The gain in the direction $\phi = 0$ are shown in Figure 7.12 for each corner angle. The solid curve in each case is computed for zero losses ($R_{1L} = 0$), while the dashed curve is for an assumed loss resistance R_{1L} = 1Ω. It is apparent that for efficient operation too small spacing should be avoided. A small spacing is also objectionable because of narrow bandwidth. On the other hand, too large a spacing results in less gain.

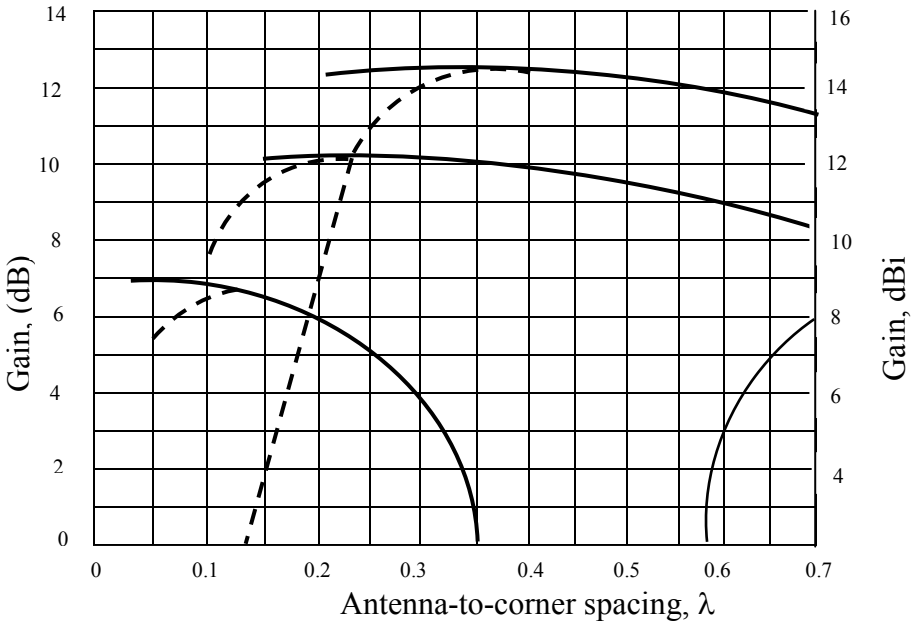

Figure 7.14 Gain of corner reflector antennas over a λ/2 dipole antenna in free space with the same power input as a function of the antenna-to-corner spacing. Gain is in the direction $\phi = 0$ and is shown for zero loss resistance (solid curves) and for an assumed loss resistance of $1\Omega\left(R_{1L} = 1\Omega\right)$ (dashed curves).

The gain of a 90° corner reflector with antenna-to-corner spacing $S \approx 0.5\lambda$ is nearly 10 dB over a reference λ/2 antenna or 12 dBi.

Restricting patterns to the lower-order radiation mode (no minor lobes), it is generally desirable that *S* lie between the following limits:

α	***S***
90°	0.25-0.7λ
180° (flat sheet)	0.1-0.3λ

In the above discussions, it is assumed that the reflectors are perfectly conducting and of infinite extent, with the exception that the gains with a finitely conducting reflector may be approximated with a proper choice of R_{1L}.

Although the gain of a corner reflector with infinite sides can be increased by reducing the corner angle, it does not follow that the gain of a corner reflector with finite sides of fixed length will increase as the corner angle is decreased. To maintain a given efficiency with a smaller corner angle requires that S be increased. Also on a 60° reflector, for example, the point at which a wave is reflected parallel to the axis is at a distance of $1.73S$ from the corner as compared to $1.41S$ for the 90^0 type. Hence, to realize the increase in gain requires that the length of the reflector sides be much larger than for a 90° corner reflector designed for the same frequency. Usually this is a practical disadvantage in view of the relatively small increase to be expected in gain.

If the length or arm of the reflector is reduced to values of less than 0.6λ, radiation to the sides and rear tends to increase and the gain decreases. When R is decreased to as little as 0.3λ, the strongest radiation is no longer forward and the "reflector" acts as a director.

7.4 PARABOLIC REFLECTOR

If a beam of parallel rays is incident upon a reflector whose geometrical shape is a parabola, the radiation will converge or get focused at a spot which is known as the *focal point*. In the same manner if a point source is placed at the focal point, the rays reflected by a parabolic reflector will emerge as a parallel beam. The symmetrical point on the parabolic surface is known as the *vertex*. Rays that emerge in a parallel formation are usually said to be *collimated*. In practice, collimation is often used to describe the highly directional characteristics of an antenna even though the emanating rays are not exactly parallel. Since the transmitter (receiver) is placed at the focal point of the parabola, the configuration is usually known as *front fed*.

A parabolic reflector can take two different forms. One configuration is that of the parabolic right cylinder, whose energy is collimated at a line that is parallel to the axis of the cylinder through the focal point of the reflector. The most widely used feed for this type of a reflector is a linear dipole, a linear array, or a slotted waveguide. The other reflector configuration is that which is formed by rotating the parabola around its axis, and it is referred to as a *paraboloid* (parabola of revolution). A pyramidal or a conical horn has been widely utilized as a feed for this arrangement.

7.4.1 Front-Fed Parabolic Reflector

Parabolic cylinders have widely been used as high-gain apertures fed by line sources. The analysis of a parabolic cylinder (single curved) reflector is similar, but considerably simpler than that of a paraboidal (double curved) reflector. The principle characteristics of aperture amplitude, phase, and polarization for a parabolic cylinder, as contrasted to those of a paraboloid, are as follows:

1. The amplitude taper, due to variations in distance from the feed to the surface of the reflector, is proportional to $1/\rho$ in a cylinder compared to $1/r^2$ in a paraboloid.
2. The focal region, where incident plane waves converge, is a line-source for a cylinder and a point source for a paraboloid.

3. When the fields of the feed are linearly polarized parallel to the axis of the cylinder, no cross-polarized components are produced by the parabolic cylinder. That is not the case for a paraboloid.

The surface of a paraboloidal reflector is formed by rotating a parabola about its axis. Its surface must be a paraboloid of revolution so that rays emanating from the focus of the reflector are transformed into plane waves. The design is based on optical techniques, and it does not take into account any deformations (diffractions) from the rim of the reflector. Referring to Figure 7.15 and choosing a plane perpendicular to the axis of the reflector through the focus, it follows that

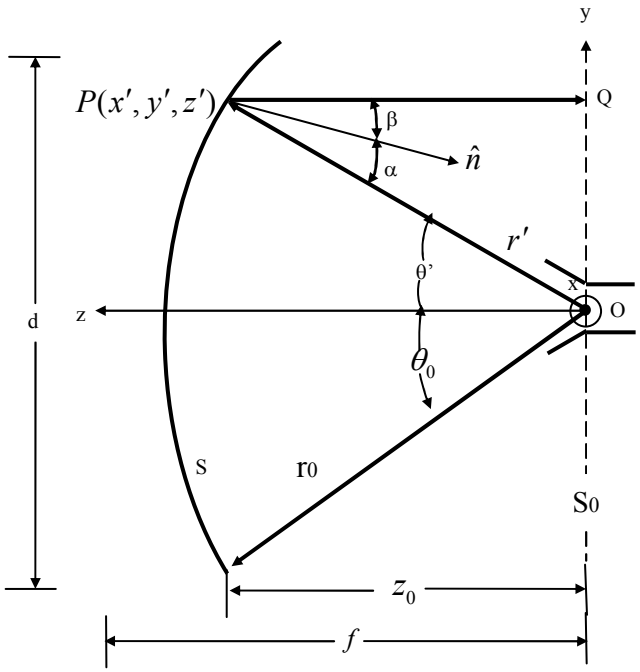

Figure 7.15 Two-dimensional configuration of a paraboloidal reflector.

$$OP + PQ = \text{constant} = 2f \tag{7.30}$$

Since

$$OP = r' \tag{7.31}$$
$$PQ = r' \cos\theta'$$

(7.30) can be written as

$$r' (1 + \cos\theta') = 2f \tag{7.32}$$

or

$$r' = \frac{2f}{1+\cos\theta'} = f \sec^2\left(\frac{\theta'}{2}\right) \quad \theta \le \theta_0 \tag{7.32a}$$

Since a paraboloid is a parabola of revolution (about its axis), (7.32a) is also the equation of a paraboloid in terms of the spherical coordinates r', θ', ϕ'. Because of its rotational symmetry, there are no variations with respect to ϕ'.

Another expression that is usually very prominent in the analysis of reflectors is that relating the subtended angle θ_0 to the *f/d* ratio. From the geometry of Figure 7.15

$$\theta_0 = \tan^{-1}\left(\frac{d/2}{z_0}\right) \tag{7.33}$$

where z_0 is the distance along the axis of the reflector from the focal point to the edge of the rim.

$$z_0 = \tan^{-1}\left|\frac{\frac{d}{2}}{f - \frac{d^2}{16f}}\right| = \tan^{-1}\left|\frac{\frac{1}{2}\left(\frac{f}{d}\right)}{\left(\frac{f}{d}\right)^2 - \frac{1}{16}}\right| \tag{7.34}$$

It can also be shown that another form of (7.34) is

$$f = \left(\frac{d}{4}\right)\cot\left(\frac{\theta_0}{2}\right) \tag{7.35}$$

Aperture antennas usually have an obvious physical aperture of area A_p through which energy passes on its way to the far field. The maximum achievable gain for an aperture antenna is

$$G_{\max} = D_u = \frac{4\pi}{\lambda^2} A_p \tag{7.36}$$

This gain is possible only under the ideal circumstances of a uniform amplitude, uniform phase antenna with no spillover or ohmic losses present. In practice, these conditions are not satisfied and gain is decreased from ideal, as represented through the following:

$$G = \varepsilon_{ap} D_u = \varepsilon_{ap} \frac{4\pi}{\lambda^2} A_p \tag{7.37}$$

It is found that for a given feed pattern

- There is only one reflector with a given angular aperture or *f/d* ratio which leads to a maximum aperture efficiency.

- Each maximum aperture efficiency is in the neighborhood of 82-83%.
- Each maximum aperture efficiency, for any one of the given patterns, is almost the same as that of any of the others.
- As the feed pattern becomes more directive, the angular aperture of the reflector that leads to the maximum efficiency is smaller.

The aperture efficiency is generally the product of the

- fraction of the total power that is radiated by the feed, intercepted, and collimated by the reflecting surface (generally known as *spillover efficiency* $\in_S$)
- uniformity of the amplitude distribution of the feed pattern over the surface of the reflector (generally known as *taper efficiency* $\in_t$)
- phase uniformity of the field over the aperture plane (generally known as *phase efficiency* $\in_p$)
- polarization uniformity of the field over the aperture plane (generally known as polarization efficiency $\in_x$)
- blockage efficiency $\in_b$
- random error efficiency $\in_r$ over the reflector surface

This in general

$$\in_{ap} = \in_s \in_t \in_p \in_x \in_b \in_r \tag{7.38}$$

An additional factor that reduces the antenna gain is the attenuation in the antenna feed and associated transmission line.

The two main factors that contribute to the aperture efficiency are the spillover and nonuniform amplitude distribution losses. Because these losses depend primarily on the feed pattern, a compromise between spillover and taper efficiency must emerge. It has been depicted pictorially in Figure 7.16.

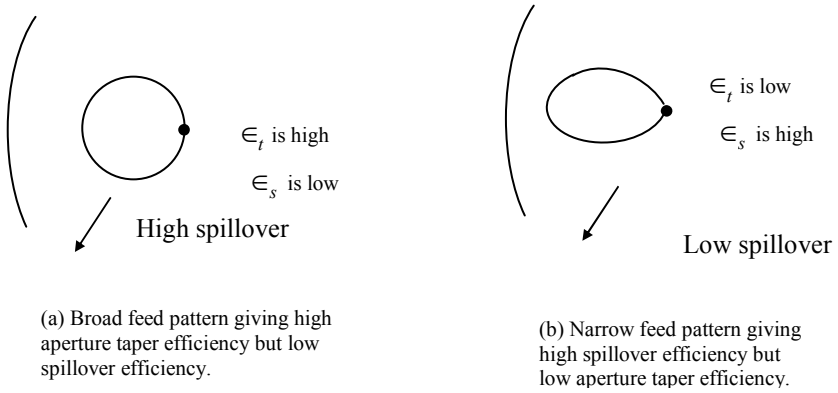

(a) Broad feed pattern giving high aperture taper efficiency but low spillover efficiency.

(b) Narrow feed pattern giving high spillover efficiency but low aperture taper efficiency.

Figure 7.16 Illustration of the influence of the feed antenna pattern on reflector aperture taper and spillover.

Very high spillover efficiency can be achieved by a narrow beam pattern with low major lobes at the expense of a very low taper efficiency. Uniform illumination and ideal taper efficiency can be obtained when the feed power pattern $G_f(\theta')$ is given by

$$G_f(\theta') = \begin{cases} \sec^4\left(\dfrac{\theta'}{2}\right) & 0 \le \theta' \le \theta_0 \\ 0 & \theta' > \theta_0 \end{cases} \tag{7.39}$$

which is plotted in Figure 5.17. Although such a pattern is "ideal" and impractical to achieve, much effort has been devoted to develop feed designs which attempt to approximate it.

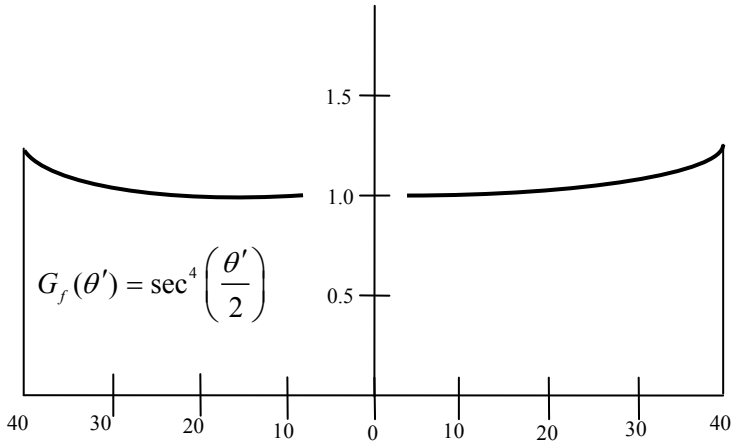

Figure 7. 17 Normalized gain pattern of feed for uniform amplitude illumination of paraboloidal reflector with a total subtended angle of 80°.

To develop guidelines for designing practical feeds which results in high aperture efficiencies, it is instructive to examine the relative field strength at the edges of the reflector's bounds ($\theta' = \theta_0$) for patterns that lead to optimum efficiencies.

In practice, maximum reflector efficiencies are in the 65-80% range. To demonstrate that paraboloidal reflector efficiencies for square corrugated horns feeds were computed and are shown in Figure 7.18(a). For the data of Figures 7.18 (a)and (b), each horn had aperture dimensions of $8\lambda \times 8\lambda$, their patterns were assumed to be symmetrical (by averaging the E- and H-planes). From the plotted data, it is apparent that the maximum aperture efficiency for each feed pattern is in the range of 74-79%, and that the product of the taper and spillover efficiencies is approximately equal to the total aperture efficiency.

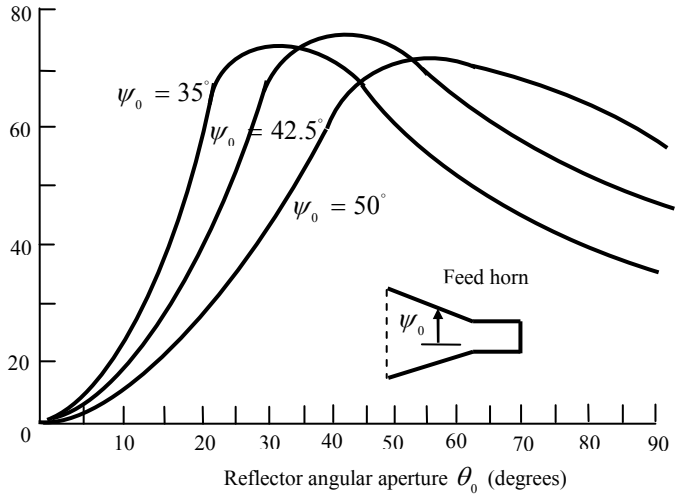

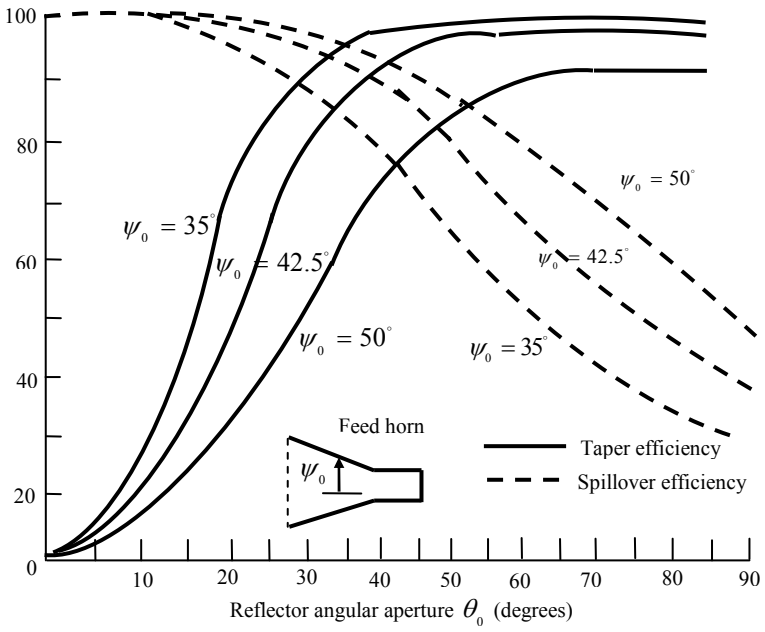

Figure 7.18 Parabolic reflector aperture efficiency as a function of angular aperture for $8\lambda \times 8\lambda$ square corrugated horn feed with total flare angles of $2\psi_0 = 70^\circ, 85^\circ$, and 100°.

Phase Errors

Any departure of the phase, over the aperture of the antenna, from uniform can lead to a significant decrease in its directivity. For a paraboloidal reflector system, phase errors result from

1. displacement (defocusing) of the feed phase center from the focal point
2. deviation of the reflector surface from a parabolic shape or random errors at the surface of the reflector
3. departure of the feed wave fronts from spherical shape

The defocusing effect can be reduced by first locating the phase center of the feed antenna and then placing it at the focal point of the reflector. It is found that the phase center for horn antennas, which are widely utilized as feeds for reflectors, is located between the aperture of the horn and the apex formed by the intersection of the inclined walls of the horn. Very simple theory has been derived to predict the loss in directivity for rectangular and circular apertures when the peak values of the aperture phase deviation is known. When the phase errors are assumed to be relatively small, it is not necessary to know the exact amplitude or phase distribution function over the aperture.

7.5 CASSEGRAIN REFLECTORS

The disadvantage of the front-fed arrangement is that the transmission line from the feed must usually be long enough to reach the transmitting or the receiving equipment, which is usually placed behind or below the reflector. This may necessitate the use of long transmission lines whose losses may not be tolerable in many applications, especially in low-noise receiving systems. In some applications, the transmitting or receiving equipment is placed at the focal point to avoid the need for long transmission lines. However, in some of these applications, especially for transmission that may require large amplifiers and for low-noise receiving systems where cooling and weatherproofing may be necessary, the equipment may be too heavy and bulky and will provide undesirable blockage.

The arrangement that avoids placing the feed (transmitter and/or receiver) at the focal point is that shown in Figure 7.1(d) and it is known as the Cassegrain feed. Through geometrical optics, Cassegrain, a famous astronomer (N. Cassegrain of France, hence its name), showed that incident parallel rays can be focused to a point by utilizing two reflectors. To accomplish this, the main (primary) reflector must be a parabola, the secondary reflector (Subreflector) a hyperbola, and the feed placed along the axis of the parabola usually at or near the vertex. Cassegrain used this scheme to construct optical telescopes, and then its design was copied for use in radio frequency systems. For this arrangement, the rays that emanate from the feed illuminate the Subreflector and are reflected by it in the direction of the primary reflector, as if they originated at the focal point of the parabola (primary reflector). The rays are then reflected by the primary reflector and are converted to parallel rays, provided the primary reflector is a parabola and the subreflector is a hyperbola. Diffraction occurs at the edges of the subreflector and primary reflector and they must be taken into account to accurately predict the overall system pattern, especially in regions of low intensity. Even in regions of high intensity, diffraction must be included if an accurate formation of the fine ripple structure of the pattern is desired. With the Cassegrain-feed arrangement, the transmitting and/or receiving equipment can be placed behind the primary reflector. This scheme makes the system relatively more accessible for servicing and adjustments.

Cassegrain designs, employing dual reflector surfaces, are used in applications where pattern control is essential, such as in satellite ground-based systems, and have efficiencies of 65-80%. They supersede the performance of the single-reflector front-fed arrangement by about 10%. Using geometrical optics, the classical Cassegrain configuration, consisting of a paraboloid and hyperboloid, is designed to achieve a uniform phase front in the aperture of the paraboloid. By employing good feed designs, this arrangement can achieve lower spillover and more uniform illumination of the main reflector. In addition, slight shaping of one or both of the dual-reflector's surfaces can lead to an aperture with almost uniform amplitude and phase with substantial enhancement in gain. These are referred to as shaped reflectors. Shaping techniques have been employed in dual-reflectors used in earth station applications.

Two reflectors with ray geometry, with concept of equivalent parabola, are shown in Figure 7.19 The use of a second reflector, which is usually referred to as the subreflector

or subdish, gives an additional degree of freedom for achieving good performance in a number of different applications. For an accurate description of its performance, diffraction techniques must be used to take into account diffractions from the edges of the subreflector, especially when its diameter is small.

In general, the Cassegrain arrangement provides a variety of benefits, such as the

1. ability to place the feed in a convenient location
2. reduction of spillover and minor lobe radiation
3. ability to obtain an equivalent focal length much greater than the physical length
4. capability for scanning and/or broadening of the beam by moving one of the reflecting surfaces

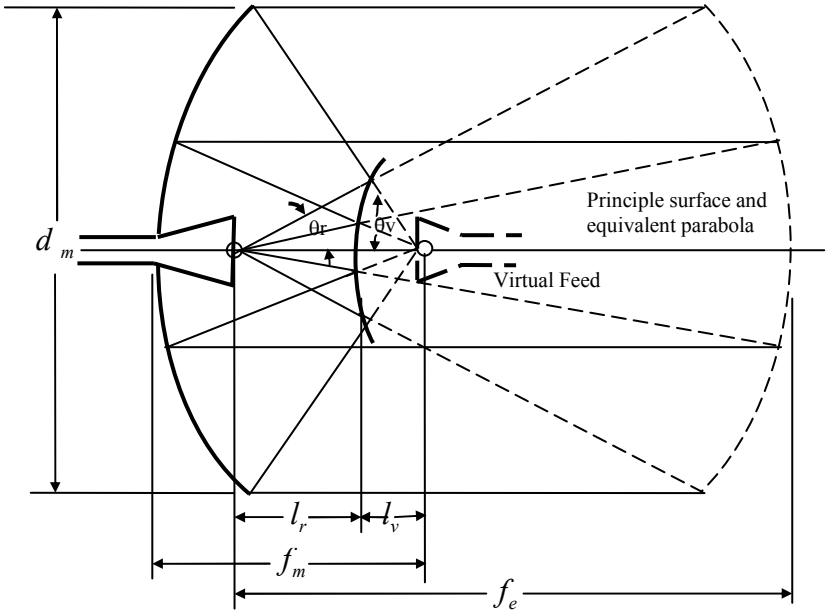

Figure 7.19 Equivalent parabola concepts.

To achieve good radiation characteristics, the subreflector must be few wavelengths in diameter. However, its presence introduces shadowing which is the principle limitation of its use as a microwave antenna. The shadowing can significantly degrade the gain of the system, unless the main reflector is several wavelengths in diameter. Therefore the Cassegrain is usually attractive for applications that require gains of 40 dB or greater. There are, however, a variety of techniques that can be used to minimize the aperture blocking by the subreflector. Some of them are minimum blocking with simple Cassegrain, and twisting Cassegrains for least blocking.

Sub-reflectors offer flexibility of design for reflecting telescopes. Referring to Figure 7.20, it is required that all rays from the focal point F form a spherical wave front (circle

of radius CF') on reflection from the (hyperbolic) subreflector (as though radiating isotropically from the parabola focus F') or by Fermat's principle of equality of path length that

$$C'A' + FA' = CA + FA \tag{7.40}$$

Noting that $CA = CF' - AF'$ and that $FA - AF' = 2OA$ we obtain

$$FA' - A'F' = 2OA = BA \tag{7.41}$$

which is the relation for an hyperbola with standard form

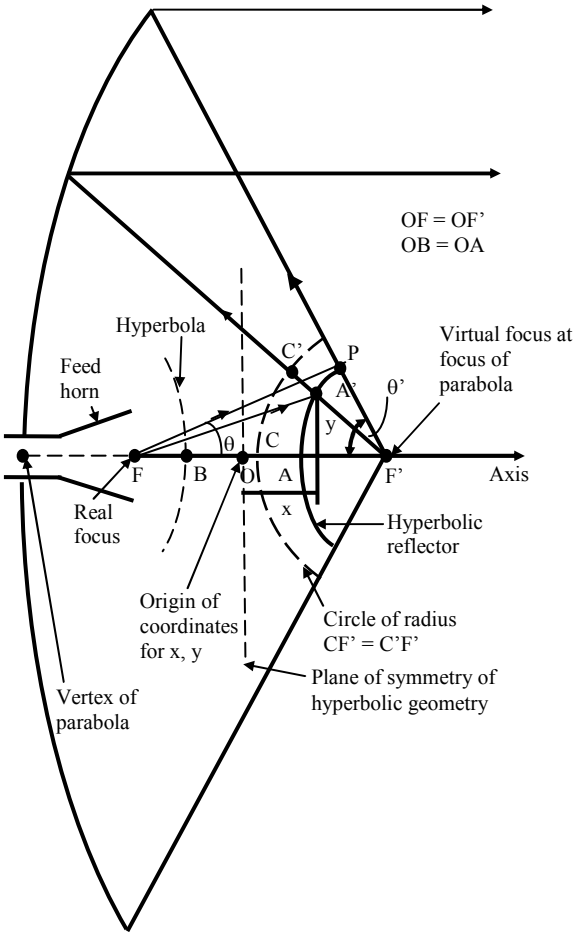

Figure 7.20 Geometry for Cassegrain reflector.

$$\frac{x^2}{a^2} - \frac{y^2}{f^2 - a^2} = 1 \tag{7.42}$$

where $a = OA = OB, f = OF' = OF$, and x and y are as shown in Figure 7.20. Or

$$y^2 = \left(\frac{x^2}{a^2} - 1\right)\left(f^2 - a^2\right) \tag{7.43}$$

The parabolic sub-reflector is then truncated at point P for which a ray reflected from the hyperbola hits the edge of the parabolic reflector. The hyperbolic reflector then subtends an angle θ from the feed location at the focal point F while the (main) parabolic reflector subtends an angle θ' from the focal point F' of the parabola. Thus, the feed horn beam angle is increased in the ratio θ'/θ to fill the parabola aperture.

The surface of the hyperbola is deformed to enlarge or restrict the incremental ray bundle, thereby decreasing or increasing the watts per steradian in the bundle and finally the watts per square meter in the aperture plane of the parabola. This shaping technique may be extended over the entire sub-reflector and often both sub-reflector and parabola are shaped. As a result a more uniform aperture distribution and higher aperture efficiency can be achieved but with higher first sidelobes and also more rapid loss as the feed is moved off-axis to squint the beam.

A constraint on the Cassegrain arrangement is that to minimize blockage the sub-reflector should be small compared to the parabola, yet the sub-reflector must be large compared to the wavelength.

In Figure 7.21 a *parabola* is given by

$$y^2 = 4fx \tag{7.44}$$

where f = focal distance = VF

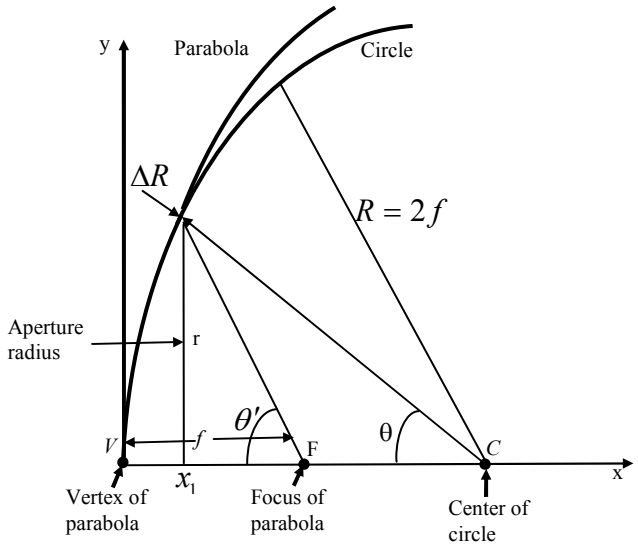

Figure 7.21 Circle and parabola compared, with radius of circle equal to twice the focal length of the parabola.

This parabola is compared with a *circle* of radius $R = VC$. It may be shown that for small values of x, the circle is of nearly the same form as the parabola when

$$R = 2f \tag{4.45}$$

Over an angle θ and *aperture radius*

$$r = R\sin\theta \tag{4.46}$$

The circle differs from the parabola by less than ΔR. If $\Delta R \ll \lambda$ (or specifically $< \lambda/16$) the field radiated from a point source at F within an angle θ' and reflected from the circle will be within $45^\circ (= 2\times 360^\circ/16)$ of the phase of a field radiated from F and reflected from the parabola. Then a feed antenna at the focal point F which illuminates the sphere only within the angle θ' will produce a plane wave over the aperture of diameter 2r having a phase deviation of less than 45°, this amount of deviation occurring only near the edge of the aperture.